SCIENTIFIC REPORTS

OPEN

SUBJECT AREAS:
THERMOELECTRICS
STRUCTURAL PROPERTIES

Received
25 September 2014

Accepted
15 December 2014

Published
14 January 2015

Correspondence and requests for materials should be addressed to Y.-H.L. lin(yh@tsinghua.edu.cn) or Q.C. (caiqing@mail.buct.edu.cn)

Enhanced thermoelectric performance of In_2O_3-based ceramics via Nanostructuring and Point Defect Engineering

Jin-Le Lan[1], Yaochun Liu[2,3], Yuan-Hua Lin[2], Ce-Wen Nan[2], Qing Cai[1] & Xiaoping Yang[1]

[1]State Key Laboratory of Organic-Inorganic Composites, Beijing University of Chemical Technology, Beijing 100029, P. R. China, [2]State Key Laboratory of New Ceramics and Fine Processing, School of Materials Science and Engineering, Tsinghua University, Beijing, 100084, P. R. China, [3]School of Materials Science and Engineering, University of Science and Technology Beijing, Beijing, 100083, P. R. China.

The issue of how to improve the thermoelectric figure of merit (*ZT*) in oxide semiconductors has been challenging for more than 20 years. In this work, we report an effective path to substantial reduction in thermal conductivity and increment in carrier concentration, and thus a remarkable enhancement in the *ZT* value is achieved. The *ZT* value of In_2O_3 system was enhanced 4-fold by nanostructuing (nano-grains and nano-inclusions) and point defect engineering. The introduction of point defects in In_2O_3 results in a glass-like thermal conductivity. The lattice thermal conductivity could be reduced by 60%, and extraordinary low lattice thermal conductivity (1.2 W m^{-1} K^{-1} @ 973 K) below the amorphous limit was achieved. Our work paves a path for enhancing the *ZT* in oxides by both the nanosturcturing and the point defect engineering for better phonon-glasses and electron-crystal (PGEC) materials.

Thermoelectric (TE) materials, which can realize direct heat-electricity conversion, have attracted extensive interests due to their widespread applications in solid-state cooling, power generation, temperature measurement, and waste heat recovery[1]. The conversion efficiency of such TE materials is generally characterized by the dimensionless figure of merit: $ZT = S^2\sigma T/(\kappa_l + \kappa_e)$, where T, S, σ, and κ_l (κ_e) are the temperature, the Seebeck coefficient, the electrical conductivity and the thermal conductivity from lattice (electrons), respectively. To date, most of the TE materials with high *ZT* values normally contain metal elements which are toxic, scarce and/or expensive (e.g., Pb, Te, Sb)[2–5]. Moreover, due to thermal instability and oxidation, these materials have limited applications at high ambient temperature for example, in waste heat utilization. In this case, oxide-based semiconductors, which are thermally and chemically stable at high temperature, have been regarded as a promising alternative. So far, among the *p*-type oxide TE materials, Co-based oxide material $Ca_3Co_4O_9$ has been intensively investigated because of its good TE performance at high temperature[6–9]. The highest *ZT* value of 0.61 at 1118 K was achieved by heavy doping and metallic nano-inclusion approach[10]. However, the *ZT* value of *n*-type TE oxides (e.g., $SrTiO_3$[11], ZnO[12], $CaMnO_3$[13]) is still lower in terms of assembling a practical oxide-based TE device due to its mediocre electrical conductivity σ (~100–200 $S.cm^{-1}$) and/or high thermal conductivity $\kappa = (\kappa_l + \kappa_e)$ (~2–10 $W.m^{-1}.K^{-1}$). In this regard, two main strategies have recently been applied to improve the *ZT*: One is to enhance the power factor ($S^2\sigma$) by tuning the carrier concentration[14], or band engineering[15–17] and the other is to reduce κ_L by enhancing phonon scattering through solid solutions and nanostructuring[2,3,18]. In fact, our previous work reveals that thermal conductivity can be reduced from 3 W m^{-1} K^{-1} (micron sample) to 2.2 W m^{-1} K^{-1} (nanostructured sample) in In_2O_3-based ceramics[19]. The nanostructurint approach results in nearly a 100% increase of *ZT* to reach 0.27 at 950 K. However, the lattice thermal conductivity cannot be reduced below 2.0 W m^{-1} K^{-1} at 950 K in the 50 nm grained sample, therefore, a substantial reduction to $\kappa_l \sim 1$ m^{-1} K^{-1} is highly desirable.

Given that phonons have a wide spectrum of wavelengths, i.e., phonons with different wavelengths contribute differently to κ_l. A variety of experiments have proved that κ_l decreases with decreasing grain size in the nanostructured thermoelectric materials, because the mean free paths for most of the phonons will be limited by the nano-grain size. Therefore, introducing the nano-grains causes mid- to long-wavelength phonons to be strongly scattered by numerous interfaces, while the short-wavelength phonons are less affected. It was shown previously that in the bulk TE materials, these short-wavelength modes can actually carry a substantial contribution of heat. For example, in a so-called all-scale (atom/nano/mesostructure) hierarchical architectures: PbTe, nearly 30% of κ_l is contributed by phonons with a wavelength of less than 5 nm, which can be attributed to scattering by atomic-scale solid-solution alloying[4]. Furthermore, for most of alloy materials, the operating temperature is in the mid-temperature range ($\sim$ 700 K) where the characteristic wavelength of heat-carrying phonons is in the order of interatomic distance. However, for the oxides those are operated at high temperature ($\sim$ 1000 K), the characteristic wavelength of phonons is always comparable to the lattice constants. The short-wavelength phonons can be scattered by introducing the point defect, resulting in a substantially reduced thermal conductivity. Zhu *et al.* found that small amount of Ge (5%) substituted in the nanostructured Si could be efficient in scattering the phonons shorter than 1 nm, resulting in a further reduction of κ_l by 50%[20].

Accordingly, to take the advantages of both point defect and nanostructuring engineering, heavy doping and spark plasma sintering (SPS) method are applied to fabricate nanostructured In_2O_3. An ultralow lattice thermal conductivity of 1.2 W m^{-1} K^{-1} @ 973 K that is below the theoretical minimum in amorphous In_2O_3 ceramics is achieved[21]. Furthermore, the observed ZT value is 4 times higher than that of pristine In_2O_3 and show the maximum value of 0.44 at 973 K, due to both the substantial reduction in thermal conductivity and the increased carrier concentration, paving a path for enhancing ZT in n-type TE oxides for high-temperature applications.

Results and Discussion

Figure 1 (a) presents the XRD patterns of all $In_{2-2x}Zn_xCe_xO_3$ specimens prepared by SPS. All of the major reflections could be well indexed to bixbyite-type cubic lattice structure with $Ia\bar{3}$ (206) space group. The existence of CeO_2 as a secondary phase was observed in the specimens for which x$>$ 0.08, suggesting that the solid solubility limit of Ce in In_2O_3 is smaller than 4%, which is larger than that of the previous report ($\sim$1%)[22]. Furthermore, it is strange that no any additional phase in XRD assignable to ZnO can be found in the patterns, since the solid solubility of Zn has been reported to be less than 2%[23]. A similar phenomenon has been reported that respective solubility can be increased greatly when the equal amounts of Zn and Sn are simultaneously cosubstituted in In_2O_3[24]. The lattice parameters of all the samples were calculated from the XRD peaks positions as shown in the Figure 1 (b). The lattice parameter increases monotonically up to x = 0.08 following Vergard formula: $a = a_0 + k\,x$, where a_0 is the pristine lattice constant and x refers to the doping level. The lattice expansion is due to the larger average ionic radius of doping species ($r_{Zn^{2+}} = 0.74$ Å, $r_{Ce^{4+}} = 0.92$ Å, $r_{ave} = 0.83$ Å) as compared to that of In^{3+} ($r_{In3+} = 0.80$ Å). The lattice parameter no longer changes as the doping level is increased beyond x = 0.08, confirming that the solubility limit is 4%.

Figure 2 shows the microstructure and phase composition of the bulk samples prepared by SPS. As observed in the high-magnification SEM (Figure 2 (a, c)), the x = 0.08, 0.12 samples exhibit nanostructure. The grain size is in the range from 20 to 100 nm, similar to our previous work for x = 0.04.[19] There are some larger grains (200–300 nm) were observed in the highly doped sample (x = 0.16) as shown in Figure S1 (a) in Supplementary Information. Based on the backscattered images (Figure 2 (d), Figure S1 (b)), it is clear that the higher doping content presents compositional inhomogeneity. However, for the lower doping level (x = 0.08), no evident mass fluctuation was observed, indicating the doping is homogeneous, which is consistent with the XRD results. In order to study the compositional variations in the sample with x = 0.16, EDX mapping was conducted for the different elements, i.e., Zn, Ce and In, as

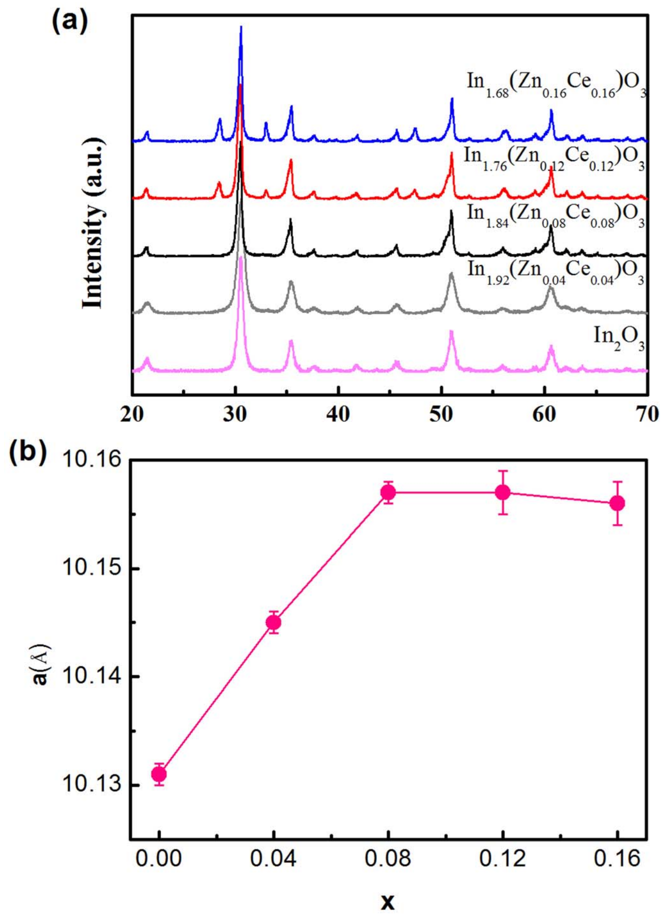

Figure 1 | (a) The XRD patterns of various $In_{2-2x}Zn_xCe_xO_3$; (b) The measured lattice parameters of $In_{2-2x}Zn_xCe_xO_3$ as a function of x.

shown in Figure S2 (b–d) in Supplementary Information. It is observed that there are Zn-rich (In-poor) and Ce-rich (In-poor) areas, which correspond to darker and brighter regions in the backscattered image, respectively. The Ce distribution seems to be more uniform, although Ce-rich inclusions also exist. The size of Zn-rich area is larger than 100 nm, which is also evident as $(ZnO)_mIn_2O_3$ compound as shown in Figure S2 (f). The composition of Ce-rich areas can be concluded to be CeO_2 phase as referred by the XRD results. Many CeO_2 nanodots (10–20 nm) were observed, which distributes homogeneously in the grain boundaries. The CeO_2 nanodots in the grain boundaries are considered to be favorable for reducing the thermal conductivity, as reported previously[25,26]. However, some of the CeO_2 inclusions in x = 0.16 samples begin to grow to be mesoscale aggregates ($\sim$100 nm), which may harm the electrical conductivity and influence the TE properties.

The temperature dependence of electrical conductivity is illustrated in Figure 3a. The electrical conductivity of all the samples decreases sharply with increasing temperature, indicating typical degenerate semiconducting transport behaviors. The room-temperature electrical conductivity increases with the doping level from 650 S cm^{-1} in the x = 0.04 sample to 1022 S cm^{-1} in the sample with x = 0.08. As the doping level is increased further, the room temperature electrical conductivity decreases sharply. This behavior is corresponding to the variety of carrier concentration with doping level as seen in the Table 1. It may be expected that the Zn^{2+}/Ce^{4+} dual doping should produce donor–acceptor pairs in In_2O_3 and give no any additional carriers as shown in Equation 1, 2. However, the significantly higher electrical conductivity ($\sim$650–1000 S cm^{-1}) of dually doped specimens than that of pristine In_2O_3 ($\sim$100 S cm^{-1}), infers that a considerable amount of carriers ($\sim$10^{19} cm^{-3}) has been

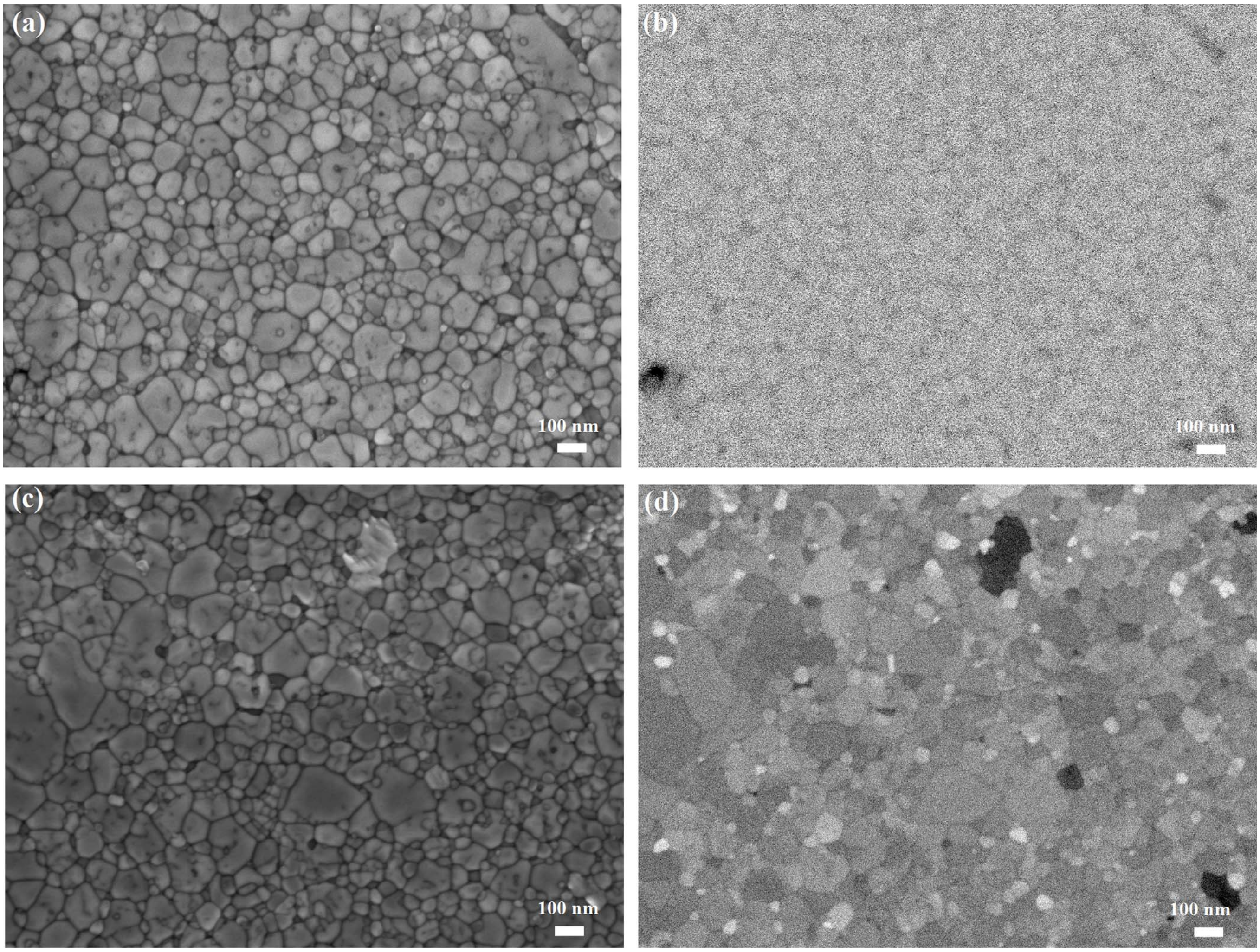

Figure 2 | High magnification SEM and BSE images of x = 0.08(a–b), x = 0.12 (c–d). The Ce-rich area corresponds to brighter region and The Zn-rich area corresponds to darker region in (d).

generated in these system. A similar phenomenon was observed in the Zn^{2+}/Sn^{4+} cosubstituted In_2O_3, and the possible explanation is the preferential loss of Zn during the preparation resulting in a Sn^{4+}/Zn^{2+} ratio greater than one, which contributes to generate the additional carriers i.e., electrons[24].

$$ZnO + \frac{1}{2}O_2\uparrow \rightarrow Zn_{In}{}' + O_o^X + h^\bullet \quad (1)$$

$$CeO_2 \rightarrow Ce_{In}{}' + \frac{3}{2}O_o^X + \frac{1}{2}O_2\uparrow + e' \quad (2)$$

Figure 3 (b) shows the Seebeck coefficient S of all the samples is negative in the whole temperature range studied, indicating n-type conduction. It is consistent with the above analysis on the electrical behaviors. Here, the temperature dependence of Seebeck coefficient is a typical type of degenerate semiconducting behavior, similar to the electrical behavior. The variation of the Seebeck coefficient for all the samples is in agreement with the variation of the carrier concentration. The materials parameter $\beta = \mu(m^*)^{3/2}/\kappa_l$ has always been used as a criterion for high performance materials, where m^* is effective density-of-states mass and μ is the carrier mobility. The effective mass is obtained by calculating the relationship between the carrier concentration and Seebeck coefficient. As given in Table 1, the effective mass does not change significantly as compared to the literature value of 0.3 m_0[27], indicating no obvious change in the band structure by dual doping. It is surprising that the sample x = 0.12 has the highest mobility. The similar mobility behavior was also observed in Nb doped $SrTiO_3$ with nano-inclusion[11]. The behavior can be partially explained by the energy filter theory that the energy barrier in the interface due to the nano-inclusion preferentially scatters the low energy electron. Meanwhile, the nano-inclusions with high surface activation can change the morphology of grains, which can contribute to the increased mobility[10,11]. Therefore, the sample x = 0.12 presents the highest material parameter β, suggesting that the electrical transport has been optimized by the nanostructuring and the point defect engineering.

The suppressed thermal conductivity caused by the point defects and nanostructures is shown in Figure 4a. The low thermal conductivity of 6.9 W m^{-1} K^{-1} at room temperature was achieved in x = 0.12, which is about 25% lower than that of the sample x = 0.04 with a grain size of 50 nm. At high temperature, the thermal conductivity is decreased from 2.8 $W.m^{-1}.K^{-1}$ in x = 0.04 to 2.1 $W.m^{-1}.K^{-1}$ in x = 0.12, which clearly shows that the effect of nano-inclusions and point defect on the phonon scattering works at high temperature, too. The total thermal conductivity κ can be expressed by the formula $\kappa = \kappa_l + \kappa_e$, where, κ_l is the lattice contribution and κ_e is the electronic one. The contribution from the electronic thermal conductivity κ_e, can be caculated from the electrical conductivity data using

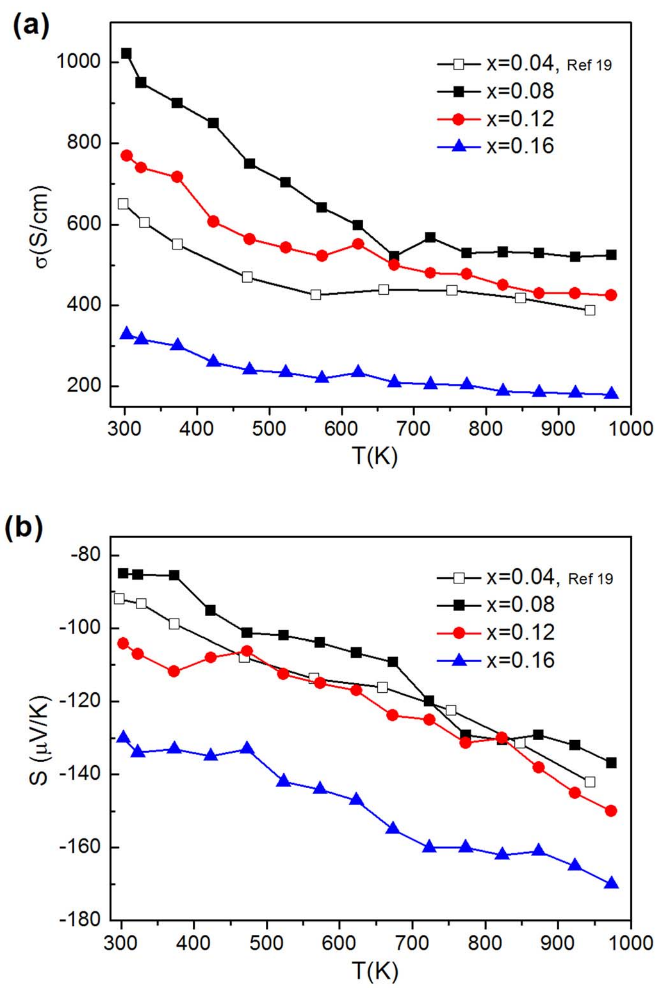

Figure 3 | Thermoelectric properties of the $In_{2-2x}Zn_xCe_xO_3$. Temperature depencences of electrical conductivity (a) and Seebeck coefficient (b).

the Wiedemann-Franz law: $\kappa_e = LT\sigma$, where, L is the Lorenz number obtained by fitting the respective Seebeck coefficient values with an estimate the reduced chemical potential (Supplementary Information, Equation 4) and σ is the electrical conductivity. The temperature dependence of κ_l for all the samples is shown in Figure 4b. The sample x = 0.12 shows the lowest κ_l at high temperature, yielding the value of 1.2 $W.m^{-1}.K^{-1}$, which is about 60% and 40% lower than that of the undoped In_2O_3 and the sample x = 0.04, respectively. This implies that the phonon scattering from the point defects and the nanostructures (including nano-grains and nano-inclusions) is an effective approach to reduce the lattice thermal conductivity of oxides at high temperature. To understand better the phonon scattering in this system, the Callaway model based on the point defect scattering is adopted to describe the influence of point defects on the lattice thermal conductivity[28,29]. The calculation results (Figure 4 (c) and details about the calculation is given in the Supplementary Information) indicate that the lattice thermal conductivity is decreased with the increasing doping level. As the results, κ_l has been reduced to 1.5 W m^{-1} K^{-1} for x = 0.16, which is about half of the value for the pristine In_2O_3. The experimentally measured κ_l values are lower than that of the theoretically calculated values, and this deviation between the measured and calculated results can be ascribed to the effect of nano-grains and nano-inclusions in the the samples x = 0.4, 0.08 and 0.12. However, for sample x = 0.16, the larger grain size of secondary phase does not play a positive role in enhancing the phonon scattering.

The so-called "amorphous limit" for thermal conductivity, k_{min} can be estimated by Cahill's formulation[21]:

$$k_{min} = \left(\frac{\pi}{6}\right)^{1/3} k_B V^{-2/3} \sum v_i \left(\frac{T}{\theta_i}\right)^2 \int_0^{\theta_i/T} \frac{x^3 e^x}{(e^x-1)^2} dx, \tag{3}$$

where, V is the average volume per atom, k_B is the Planck constants, θ_i is the Debye temperature of each polarization. The k_{min} (as shown in Figure 4 (b)) of In_2O_3-based compounds can be calculated as 0.9 $W.m^{-1}.K^{-1}$ and 1.2 $W.m^{-1}.K^{-1}$ at the temperature of 327 K and 973 K, respectively. It should be noted that the measured κ_l of x = 0.12 is lower than the calculated k_{min}, indicating this material is closed to being a phonon-glass and electron crystals.

Many efforts have been made to increase the *ZT* value of TE materials, and one of the most effective methods used is to reduce the thermal conductivity by grain boundary scattering through nanostructuring methods. However, decreasing the grain sizes always leads to a great reduction in the electrical conductivity by the increased energy barrier, which is not favorable for enhancing the *ZT* values. Therefore, all-scale hierarchical architectures have been proposed to maximize the reduction in lattice thermal conductivity and retain the high electrical properties[4]. In order to retain the electrical conductivity, the mesoscale grains should be connected together to form a fast electron transport pathway, and numerous interface by the nanostructure to enhance the phonon scattering, which is proposed by Zhao et al[30]. The carrier and phonon transport paths in the x = 0.12 is helpful to effectively scatter phonons on the multiple length scale (nanoscale and mesoscale). Furthermore, the point defect enhances the carrier concentration and suppress the atomic-scale scattering, therefore the sample x = 0.12 achieved the highest *ZT*.

The *ZT* value is improved to 0.44 at 923 K for x = 0.12 as shown in Figure 5 (a). The ZT value of In_2O_3 was enhanced 4-fold by Zn and Ce dual doping as compared to that of the pristine sample, and is about 60% higher than that of the sample x = 0.04. Additionally, this *ZT* value is higher than that of the other oxide systems, *i.e.* $SrTiO_3$[31], ZnO[12] and $CaMnO_3$[13] as shown in the Figure 5b.

In summary, our work on heavily doped In_2O_3 nanostructured ceramics demonstrates that modulating point defects improve the electrical conductivity and suppress the lattice thermal conductivity, simultaneously. The lattice thermal conductivity has been reduced by 60%, and the minimum lattice thermal conductivity (1.2 W m^{-1} K^{-1} @ 973 K) can be reached to the theoretical minimum or amorphous limit. Hence, the highest *ZT* value of 0.44 at 973 K makes In_2O_3-based bulk ceramics a promising candidate for thermoelectric power generation applications. Our work not only deals with the higher ZT

Table 1 | Seebeck coefficient (*S*), Carrier concentration (*n*), carrier mobility (μ), the effective mass (m^*) and the Lorenz number (*L*) at room temperature for various $In_{2-x}Zn_xCe_xO_3$

Nominal composition	S ($\mu V K^{-1}$)	n (10^{19} cm^{-3})	μ ($cm^2V^{-1}s^{-1}$)	m^* (m_0)	L (10^{-8} V^2K^{-2})
x = 0.04	92	5.05	81.3	0.33	2.33
x = 0.08	85	7.04	91.3	0.36	2.34
x = 0.12	104	4.21	114.6	0.33	2.31
x = 0.16	130	2.92	70.7	0.34	2.30

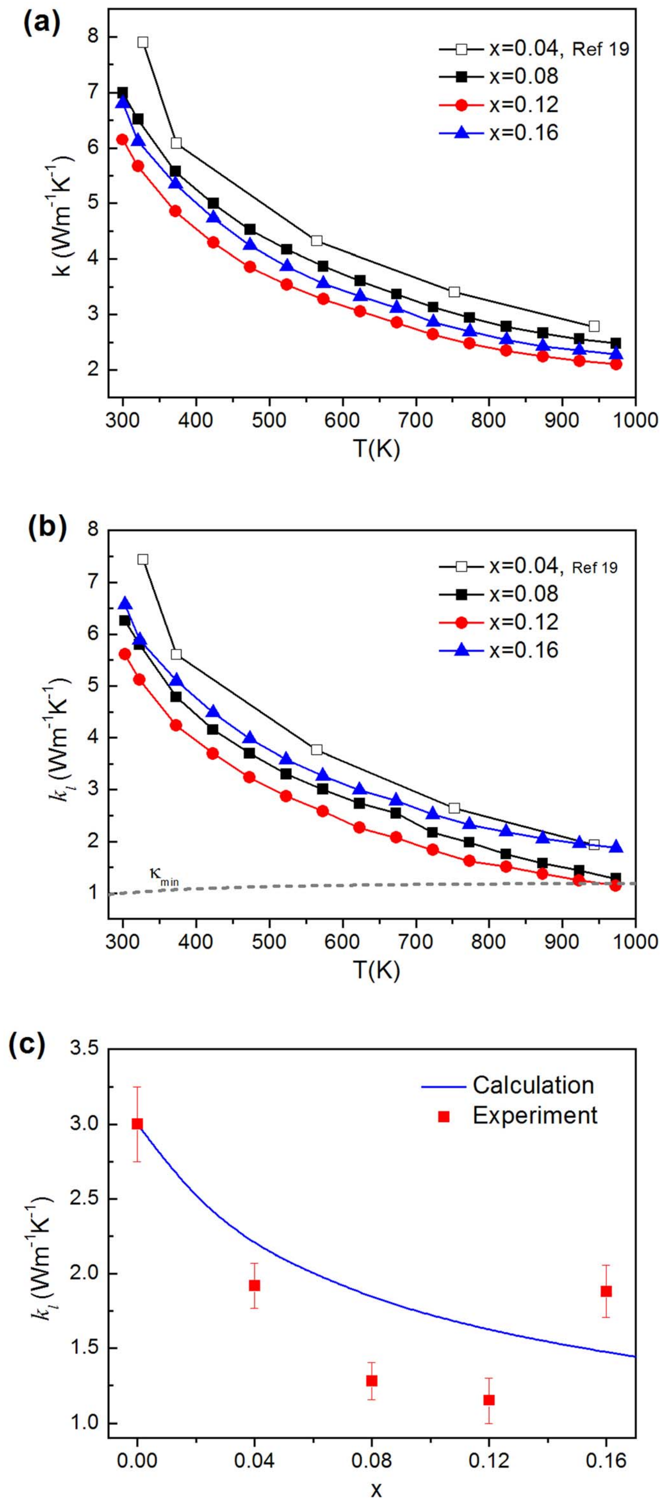

Figure 4 | Temperature dependence of (a) Total thermal conductivity and (b) Lattice thermal conductivity using the calculated Lorenz number, of various $In_{2-2x}Zn_xCe_xO_3$. The dash line is calculated minimum lattice thermal conductivity. (c) Lattice thermal conductivity of various $In_{2-2x}Zn_xCe_xO_3$ at 973 K as a function of x. The solid line is the caculated lattice thermal conductivity used the Callaway model.

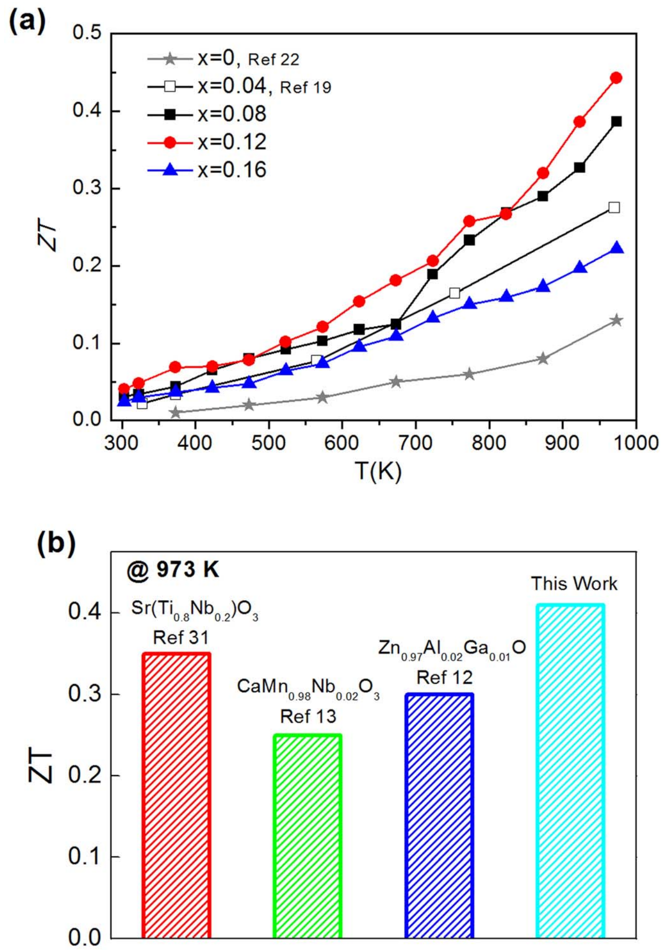

Figure 5 | (a) Temperature dependence of *ZT* for $In_{2-2x}Zn_xCe_xO_3$. (b) *ZT* values at 973 K of the present work and other reported polycrystalline oxide TE materials.

in In_2O_3 based system but also provides a systematic ground for improving the performance of other ceramic-based TE materials.

Methods

Sample preparation. $InCl_3$, $Zn(NO_3)_2$, $Ce(NO_3)_3 \cdot 6\ H_2O$, and NH_4HCO_3 were dissolved in distilled water to make the nitrate stock solution. The resultant suspension was subjected to suction filtration. The filtrate was washed with distilled water before drying at 343 K for 2 h. The precursor powder was calcined at 623 K for 2 h in air. The obtained powder was then pressed and sintered at 1153 K by using Spark Plasma Sintering (SPS) method. The density for all the samples could reach up to ~95% of the theoretical density.

Sample characterization. X-ray diffraction (XRD) with a Rigaku D/MAX-2550V diffractometer (Rigaku, Japan; Cu Kα radiations) and high resolution scanning electron microscopy (FE-SEM, Carl Zeiss Merlin with a 0.8 nm resolution) were employed to study the phase composition and microstructures, respectively. The samples for SEM and BSE observation were carefully polished and then thermally etched at 1053 K for half an hour. The samples for the measurements of thermoelectric properties were cut out of the sintered bodies in the form of rectangular bars of 3 mm by 3 mm by 15 mm with a diamond blade, and then silver paint electrodes were formed on both sides of the sintered ceramic discs for electrical measurements. The electrical conductivity and Seebeck coefficient were measured by commercial equipment (Ulvac, ZEM-3). The high-temperature thermal conductivity κ was determined from measurements of the thermal diffusivity (α), the heat capacity (C_p), and the density (ρ), using the relationship: $\kappa = \alpha \times C_p \times \rho$. The relative bulk density was measured by the Archimedes method. A Netzsch LFA 457 laser flash apparatus measured the thermal diffusivity and the specific heat. The Hall coefficients were measured using the Vander Pauw technique under a magnetic field of 0.7 T. The estimated measurement accuracies are listed below for the commercial equipments used: 5% for the electrical resistivity, 7% for the Seebeck coefficient, 10% for the specific heat, and 5% for the thermal diffusivity.

1. Bell, L. E. Cooling, Heating, Generating Power, and Recovering Waste Heat with Thermoelectric Systems. *Science* **321**, 1457–1461 (2008).
2. Poudel, B. *et al.* High-Thermoelectric Performance of Nanostructured Bismuth Antimony Telluride Bulk Alloys. *Science* **320**, 634–638 (2008).
3. Mehta, R. J. *et al.* A new class of doped nanobulk high-figure-of-merit thermoelectrics by scalable bottom-up assembly. *Nat Mater* **11**, 233–240 (2012).

4. Biswas, K. *et al.* High-performance bulk thermoelectrics with all-scale hierarchical architectures. *Nature* **489**, 414–418 (2012).
5. Wu, H. J. *et al.* Broad temperature plateau for thermoelectric figure of merit ZT> 2 in phase-separated $PbTe_{0.7}S_{0.3}$. *Nat. Commun.* **5**, 4515 (2014).
6. Wang, Y., Sui, Y., Cheng, J., Wang, X. & Su, W. Comparison of the high temperature thermoelectric properties for Ag-doped and Ag-added $Ca_3Co_4O_9$. *J. Alloy. Compd.* **477**, 817–821 (2009)
7. Noudem, J. G., Kenfaui, D., Chateigner, D. & Gomina, M. Toward the enhancement of thermoelectric properties of lamellar $Ca_3Co_4O_9$ by edge-free spark plasma texturing. *Scripta. Mater.* **66**, 258–260 (2012).
8. Liu, Y., Lin, Y., Shi, Z., Nan, C.-W. & Shen, Z. Preparation of $Ca_3Co_4O_9$ and Improvement of its Thermoelectric Properties by Spark Plasma Sintering. *J. Am. Ceram. Soc.* **88**, 1337–1340 (2005).
9. Liu, H. Q., Song, Y., Zhang, S. N., Zhao, X. B. & Wang, F. P. Thermoelectric properties of $Ca_{3-x}Co_4O_{9+\delta}$ ceramics. *J. Phys. Chem. Solids.* **70**, 600–603 (2009).
10. Van Nong, N., Pryds, N., Linderoth, S. & Ohtaki, M. Enhancement of the Thermoelectric Performance of p-Type Layered Oxide $Ca_3Co_4O_{9+\delta}$Through Heavy Doping and Metallic Nanoinclusions. *Adv. Mater.* **23**, 2484–2490 (2011).
11. Wang, N. *et al.* Enhanced thermoelectric performance of Nb-doped $SrTiO_3$ by nano-inclusion with low thermal conductivity. *Sci. Rep.* **3**, 3449 (2013).
12. Brockway, L., Vasiraju, V., Sunkara, M. K. & Vaddiraju, S. Engineering Efficient Thermoelectrics from Large-Scale Assemblies of Doped ZnO Nanowires: Nanoscale Effects and Resonant-Level Scattering. *ACS Appl. Mater. Interfaces.* **6**, 14923–14930 (2014).
13. Bocher, L. *et al.* $CaMn_{1-x}Nb_xO_3$ ($x \leq 0.08$) Perovskite-Type Phases As Promising New High-Temperature n-Type Thermoelectric Materials. *Inorg. Chem.* **47**, 8077–8085 (2008).
14. Snyder, G. J. & Toberer, E. S. Complex thermoelectric materials. *Nat. Mater.* **7**, 105–114 (2008).
15. Heremans, J. P. *et al.* Enhancement of Thermoelectric Efficiency in PbTe by Distortion of the Electronic Density of States. *Science* **321**, 554–557 (2008).
16. Pei, Y. *et al.* Convergence of electronic bands for high performance bulk thermoelectrics. *Nature* **473**, 66–69 (2011).
17. Zhang, Q. *et al.* Enhancement of thermoelectric figure-of-merit by resonant states of aluminium doping in lead selenide. *Energy. Environ. Sci.* **5**, 5246–5251 (2012).
18. Li, Z.-Y. & Li, J.-F. Fine-Grained and Nanostructured $AgPb_mSbTe_{m+2}$ Alloys with High Thermoelectric Figure of Merit at Medium Temperature. *Adv. Energy Mater.* **4**, 1300937 (2014).
19. Lan, J., Lin, Y.-H., Liu, Y., Xu, S. & Nan, C.-W. High Thermoelectric Performance of Nanostructured In_2O_3-Based Ceramics. *J. Am. Ceram. Soc.* **95**, 2465–2469 (2012).
20. Zhu, G. H. *et al.* Increased Phonon Scattering by Nanograins and Point Defects in Nanostructured Silicon with a Low Concentration of Germanium. *Phys. Rev. Lett.* **102**, 196803 (2009).
21. Cahill, D. G., Watson, S. K. & Pohl, R. O. Lower limit to the thermal conductivity of disordered crystals. *Phys. Rev. B.* **46**, 6131–6140 (1992).
22. Liu, Y. *et al.* High-Temperature Transport Property of $In_{2-x}Ce_xO_3$ ($0 \leq x \leq 0.10$) Fine Grained Ceramics. *J. Am. Ceram. Soc.* **95**, 2568–2572 (2012).
23. Moriga, T. *et al.* Phase Relationships and Physical Properties of Homologous Compounds in the Zinc Oxide-Indium Oxide System. *J. Am. Ceram. Soc.* **81**, 1310–1316 (1998).
24. Palmer, G. B., Poeppelmeier, K. R. & Mason, T. O. Conductivity and Transparency of ZnO/SnO_2-Cosubstituted In_2O_3. *Chem. Mater.* **9**, 3121–3126 (1997).
25. Kim, W. *et al.* Reducing Thermal Conductivity of Crystalline Solids at High Temperature Using Embedded Nanostructures. *Nano. Lett.* **8**, 2097–2099 (2008).
26. He, J. *et al.* On the Origin of Increased Phonon Scattering in Nanostructured PbTe Based Thermoelectric Materials. *J. Am. Chem. Soc.* **132**, 8669–8675 (2010).
27. Guilmeau, E. *et al.* Tuning the transport and thermoelectric properties of In_2O_3 bulk ceramics through doping at In-site. *J. Appl. Phys.* **106**, 053715 (2009).
28. Callaway, J. & von Baeyer, H. C. Effect of Point Imperfections on Lattice Thermal Conductivity. *Phys. Rev.* **120**, 1149–1154 (1960).
29. Pei, Y.-L. *et al.* High thermoelectric performance of oxyselenides: intrinsically low thermal conductivity of Ca-doped BiCuSeO. *NPG Asia Mater* **5**, e47 (2013).
30. Zhao, L.-D., Zhang, B.-P., Liu, W.-S. & Li, J.-F. Effect of mixed grain sizes on thermoelectric performance of Bi_2Te_3 compound. *J. Appl. Phys.* **105**, 023704 (2009).
31. Ohta, S., Ohta, H. & Koumoto, K. Grain Size Dependence of Thermoelectric Performance of Nb-Doped $SrTiO_3$ Polycrystals. *J. Ceram. Soc. Jpn.* **114**, 102–105 (2006).

Acknowledgments

This work was financially supported by the Ministry of Sci& Tech of China through a 973-Project, under grant No. 2013CB632506, NSF of China under Grant No. 51025205, 51402010 and 11234012, and Specialized Research Fund for the Doctoral Program of Higher Education, under grant No. 20120002110006.

Author contributions

J.-L.L. designed the experiments. J.-L.L. carried out the fabrication of materials and thermoelectric measurements. J.-L.L. and Y.C.L. contributed to microstructural characterizations. C.-W.N., Q.Y. and Q.C. provided helps in the experiments. J.-L.L. and Y.-H.L. wrote the paper, and all authors reviewed the manuscript.

Additional information

Supplementary information accompanies this paper at http://www.nature.com/scientificreports

Competing financial interests: The authors declare no competing financial interests.

How to cite this article: Le Lan, J.- *et al.* Enhanced thermoelectric performance of In_2O_3-based ceramics via Nanostructuring and Point Defect Engineering. *Sci. Rep.* **5**, 7783; DOI:10.1038/srep07783 (2015).